CHAPTER IV
RESULTS AND DISCUSSION

4.1 Chemical Structure of Chitosan and Hexanoyl Chitosan

Chitosan employed as the starting material had 91% degree of deacetylation and a viscosity-average molecular weight of 3.72×10^5 g/mol. The FT-IR spectrum of chitosan is shown in Figure 4.1 (a). The characteristic absorption peaks of chitosan were observed at 3000~4000 cm^{-1} (OH, NH_2), 2867 cm^{-1} (-CH- stretching),1655 cm^{-1} (-CONH-, amide I), 1554 cm^{-1} (-NH, amide II), 1317 cm^{-1} (C-N stretching), and 1107 cm^{-1} (C-O stretching vibration).

Figure 4.1 (b) shows the FT-IR spectrum of H-chitosan. The characteristic absorption peaks of H-chitosan were observed at 1716 cm^{-1} (C=O of N $(COR)_2$), 1745 cm^{-1} (C=O of OCOR), 2958 cm^{-1}(ν_{as} CH_3), 2932 cm^{-1} ($\nu_{as}CH_2$), 2872 cm^{-1} (ν_s CH_2), 1471 cm^{-1} ($\delta_s CH_2$), and 1164 cm^{-1} (twisting vibration of CH_2).

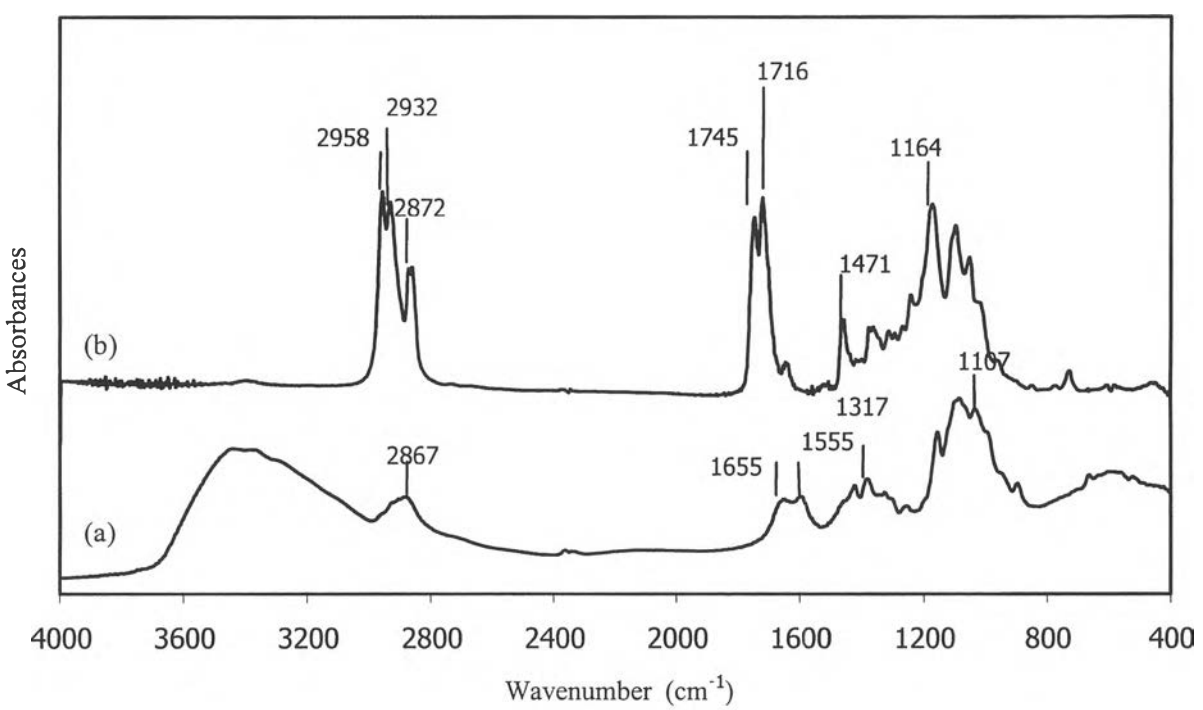

Figure 4.1 FT-IR spectra of (a) chitosan and (b) H-chitosan.

The characteristic absorption peaks of chitosan which were observed at 3000~4000 cm^{-1} were absent in the FT-IR spectrum of H-chitosan, indicating that hexanoylation reaction occurred at the hydroxyl groups of chitosan. The FT-IR analysis suggests that hexanoyl groups substituted into hydroxyl and amino groups on the monosaccharide of chitosan.

^{1}H-NMR and ^{13}C-NMR were used to confirm the chemical structure of H-chitosan. ^{1}H-NMR spectrum of H-chitosan in $CDCl_3$ (Figure 4.2) shows signals at 5.6(H1), 5.2 (H3), 4.2 (H4), 3.4~3.6 (H6, H5), and 2.6 (H2) ppm due to the protons of the polysaccharide ring and the signals at 2.4 (-CO-CH_2-), 1.3-1.6 (-CH_2-), and 0.9 (-CH_3) ppm which are assigned to the peaks of hexanoyl chains.

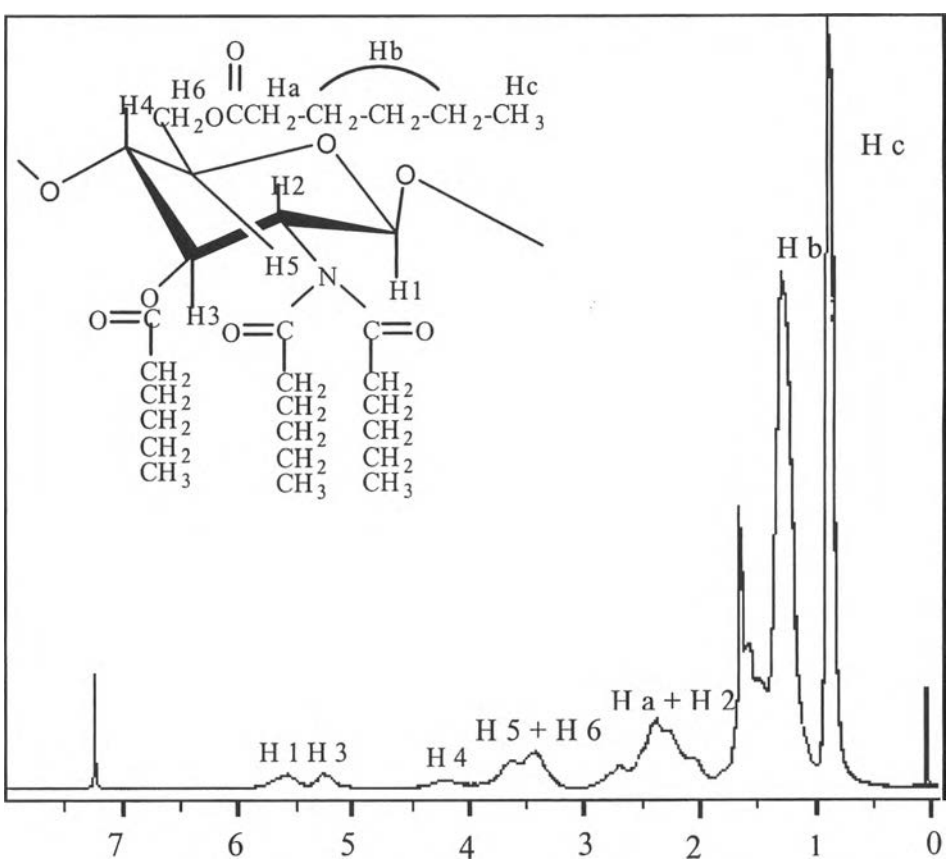

Figure 4.2 ^{1}H-NMR spectrum of H-chitosan.

Figure 4.3 illustrates ^{13}C-NMR spectrum of H-chitosan in $CDCl_3$. The signals were observed at 58 (C2), 6.5 (C4), 73 (C3), and 99 (C1) ppm which are attributed to the carbons in the polysaccharide ring. The signals of β-ε carbons of hexanoyl groups are shown at 14 (a), 22.4 (b), 31.3 (c), and 24.4 (d) ppm as singlet

signals while the signals of α-CH_2 are split into 7 peaks at 27.1, 28.2, 29.6, 33.8, 36.0, and 39.5 ppm corresponding to the hexanoyl groups in different environment. The signals shown at 178.7, 176.5, 172.5, 171, 168.6, and 165.5 ppm are assigned to the carbonyl carbons. Similar results have been reported by Zong *et al.* (2000), who synthesized and characterized the structures of acylated chitosan.

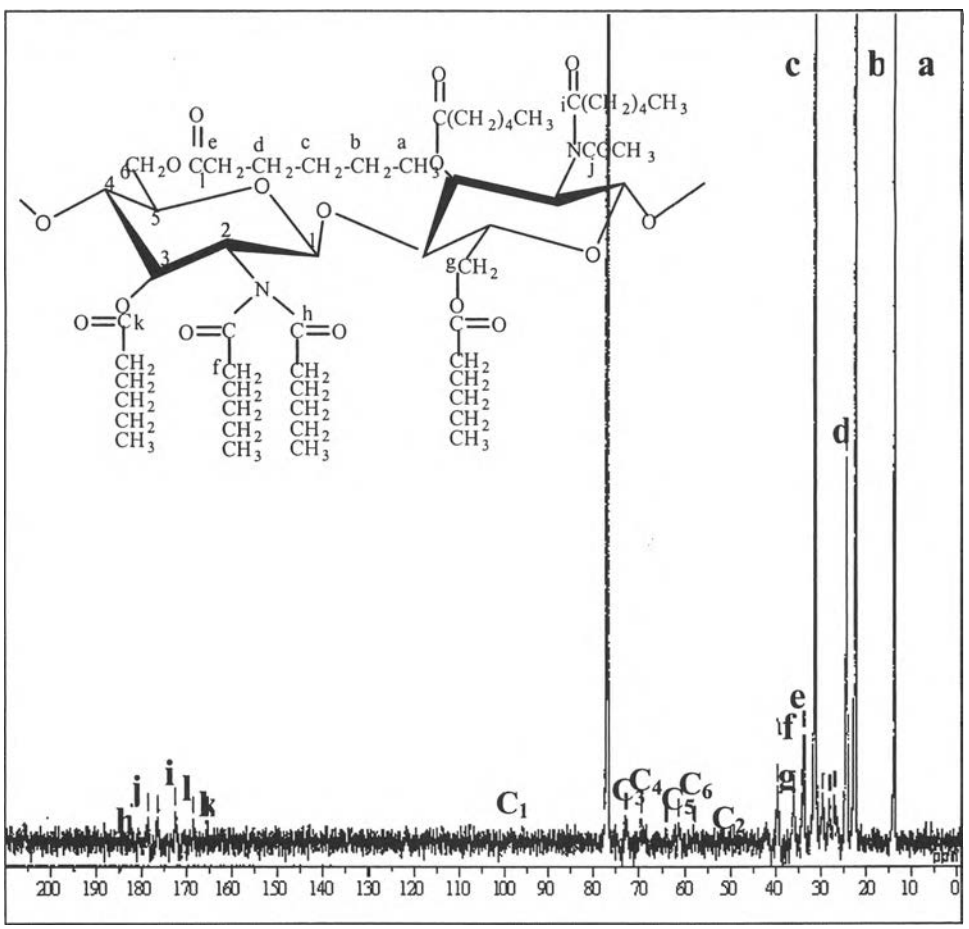

Figure 4.3 ^{13}C-NMR spectrum of H-chitosan.

From FT-IR, ^{1}H-NMR, and ^{13}C-NMR analysis, the results indicate that H-chitosan was obtained after the chemical modification of chitosan by hexanoylation reaction.

4.2 Chemical Structure of H-chitosan/PCL Blend films

Blend films of H-chitosan and PCL with various blend compositions were prepared using chloroform as co-solvent. To obtain information on the interaction between the polymers, the chemical structures of pure H-chitosan, PCL, and H-chitosan/PCL blend films were investigated by FT-IR spectrometer. As shown in Figure 4.4 (a) the FT-IR spectrum of hexanoyl chitosan (H-chitosan) has the characteristic peaks at 1716 cm^{-1} (C=O of N $(COR)_2$), 1745 cm^{-1} (C=O of OCOR), and 2958 cm^{-1}(ν_{as} CH_2), 2932 cm^{-1} (ν_{as} CH_2), 2872 cm^{-1} (ν_s CH_2), 1471 cm^{-1} (δ_s CH_2), and 1164 cm^{-1} (twisting vibration of CH_2).

For pure PCL film (Figure 4.4 (f)), the carbonyl stretching absorbance (C=O of OCOR) was observed at about 1722 cm^{-1} and 1732 cm^{-1}, which correspond to the crystalline and amorphous components, respectively. The other peaks appear at 2945 cm^{-1} (ν_{as} CH_2), 2864 cm^{-1} (ν_s CH_2), 1471 cm^{-1} ($\nu_{as}CH_2$), 1190 cm^{-1} (O-C-C $\nu_{as}CH_2$), 1108 cm^{-1} (C-O stretching), and 732 cm^{-1} (C-C stretching).

The FT-IR spectra of H-chitosan/PCL blend films with various blend compositions (Figure 4.4 (b)-(e)) exhibit the characteristic peaks of both pure H-chitosan and PCL. There is no additional peak for interaction between α-H atoms of hexanoyl groups and carbonyl groups of PCL. This result indicates that the interaction might be quite weak and could not be detected by using FT-IR technique. De Kesel *et al.* (1999) studied the miscibility of PCL/poly(vinyl alcohol) (PVA) blends by using DSC, FT-IR, and optical microscopy. The FT-IR results indicated that no change of carbonyl absorption of PCL was observed and the hydrogen bond between PCL and PVA in the OH region was difficult to detect. This might indicated that the hydrogen bond between PCL/PVA is quite weak.

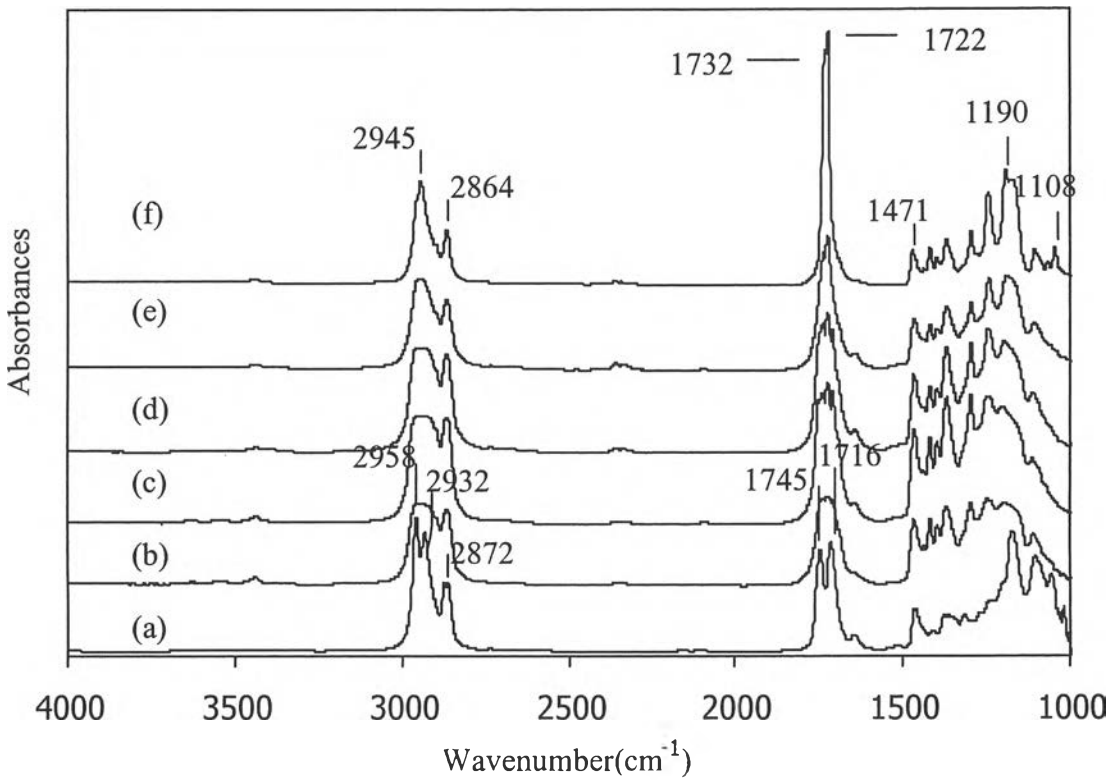

Figure 4.4 FT-IR spectra of H-chitosan/PCL blend films. H-chitosan/PCL blend composition; (a) 100/0 (H-chitosan); (b) 80/20; (c) 60/40; (d) 40/60; (e) 20/80; and (f) 0/100 (PCL).

4.3 Morphology

The surface morphology of H-chitosan/PCL blend films was characterised by using SEM. Before etching the surface of blend films, the surface morphology was difficult to observe the dispersed phase. However, when the surface of blend films was etched the dispersed phase was readily observed, as shown in Figure 4.5 (b)-(e). Figure 4.5 (a) shows a smooth surface of pure H-chitosan film. In contrast, pure PCL film (Figure 4.5 (f)) shows many voids on the surface. The similar result was reported by Ng *et al.* (2000) who investigated surface morphology of PCL film by atomic force microscopy. The film was fabricated using solution casting technique and methylenechloride was used as a solvent. They found that the voids were observed on the surface of in PCL film. Huatan *et al.* (1995) reported that PCL microspheres made from solvent evaporation techniques were porous in nature and

the porosity might be attributed to the presence of surface imperfections and high crystallization rate of PCL.

Figures 4.5 (b) and (c) show SEM micrographs of H-chitosan/PCL blend films with blend compositions of 80/20 and 60/40, respectively. The presence of voids could be observed for the blend films after it was immersed in acetic acid solution to remove PCL. According to this, the etched film contained voids which corresponded to the positions of PCL particles. It could be observed that PCL particles were regularly dispersed throughout the H-chitosan matrix. In addition, the sizes of voids became larger when PCL content increased from 20% to 40%. The surface morphology of H-chitosan/PCL blend films with blend compositions of 40/60 and 20/80 are shown in Figures 4.5 (d) and (e), respectively. The presence of voids was observed for the blend films after immersing in cyclohexane to remove H-chitosan. The etched film had voids which represented to the position of H-chitosan particles. It could be observed that the void sizes were not noticeably changed when H-chitosan content was increased from 20% to 40%.

From SEM technique, the etched surface morphology of H-chitosan/PCL blend films indicates that the phase separation occurred in all the blend compositions.

Similar observations were reported by Olabarrieta *et al.* (2001) who prepared chitosan/PCL blend films with 5, 10, and 15% (w/w) of PCL content and investigated the fracture surface morphology of these blend films. It was revealed that chitosan/PCL blend which containing 15% (w/w) of PCL content showed ellipsoidal PCL particles dispersed in chitosan matrix and the particles were small (1-10 μm). They concluded that phase separation occurred in chitosan and PCL blend. Kim *et al.* (2000) investigated the morphology of PCL/corn starch granules blends. It was found that corn starch granules dispersed in the PCL matrix. This indicated that phase separation occurred in PCL/corn starch granules blends.

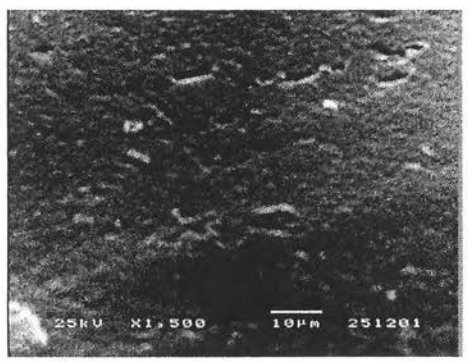

(a)

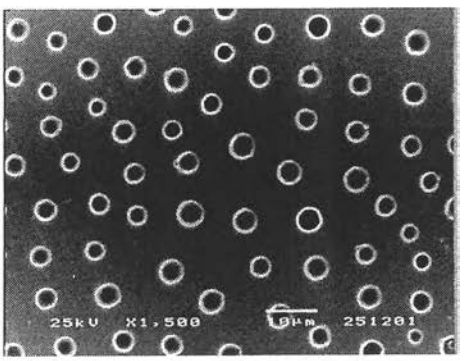

(b)

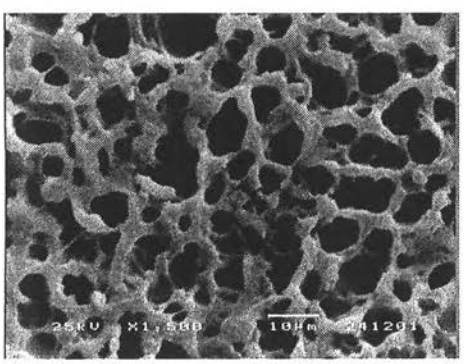

(c)

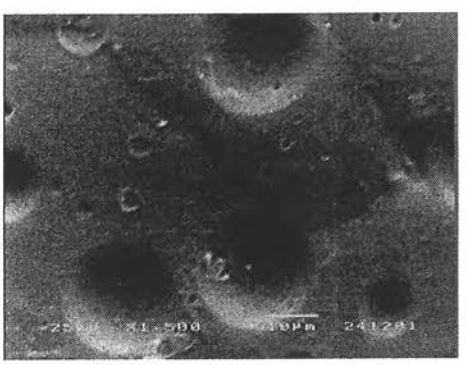

(d)

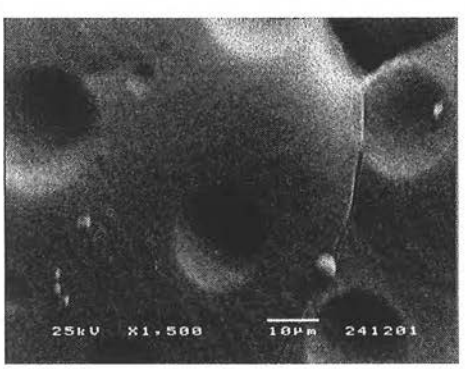

(e)

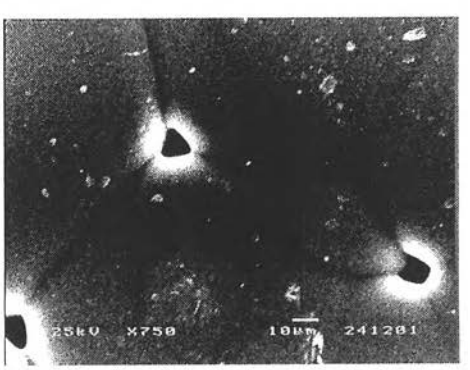

(f)

Figure 4.5 SEM micrographs of H-chitosan/PCL blend films. H-chitosan/PCL blend composition: (a) 100/0 (H-chitosan); (b) 80/20; (c) 60/40; (d) 40/60; (e) 20/80; and (f) 0/100 (PCL).

4.4 Miscibility

The miscibility of H-chitosan/PCL blend films was evaluated by focusing on the shift of glass transition temperature (T_g) of the blend films compared to those of the pure components. For pure H-chitosan, the DSC thermogram is shown in Figure 4.6 (a). It was found that no obvious T_g for H-chitosan was observed. Zong *et al.* (2000) studied thermal properties of chitosan, H-chitosan, decanoyl chitosan (D-chitosan), and lauroyl chitosan (L-chitosan) by DSC measurement. The T_g of D-chitosan and L-chitosan was detected at –43°C and -37°C, respectively, but no obvious T_g was observed for H-chitosan. DSC thermogram of pure PCL is presented in Figure 4.6 (d). It exhibits T_g at –63.5°C and an endothermic peak attributed to the melting temperature (T_m) at 63.8°C. Therefore, only T_g and T_m of PCL were detected for DSC thermograms of the blend films (Figure 4.6 (b) and (c)).

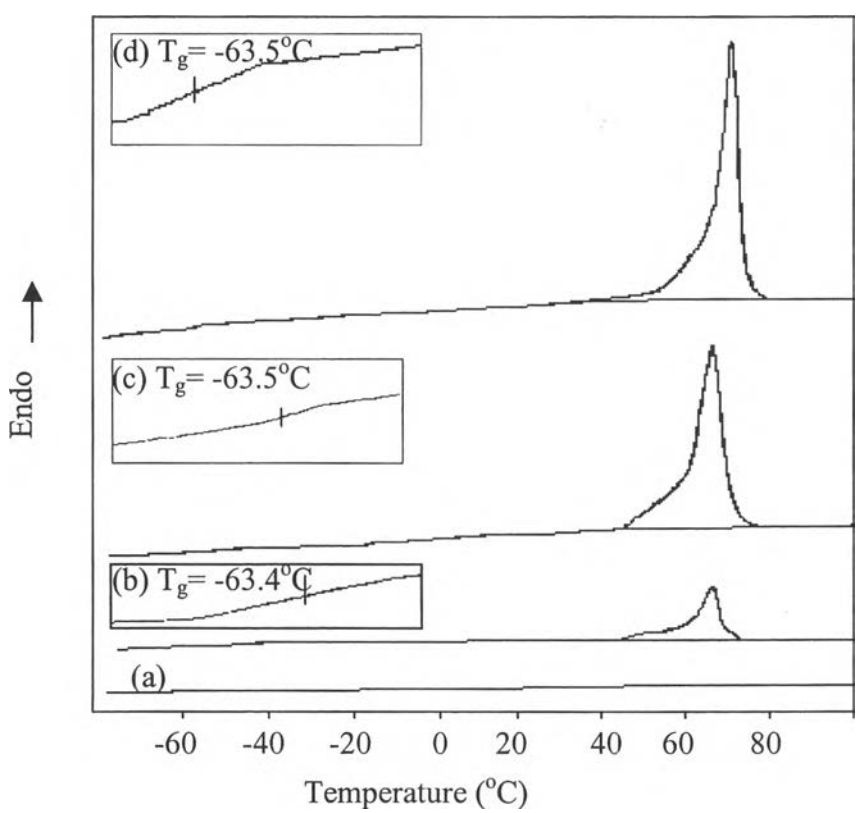

Figure 4.6 DSC thermograms of H-chitosan/PCL blend films. H-chitosan/PCL blend composition: (a) 100/0 (H-chitosan); (b) 40/60; (c) 60/40; and (d) 0/100 (PCL).

Figure 4.7 exhibits T_g of blend films as a function of H-chitosan content. The result shows that there was no obvious changed in T_g of the blend films when H-chitosan content was increased. Figure 4.8 shows T_m of blend films as a function of H-chitosan content. It was found that T_m of blend films did not remarkably change when H-chitosan content was increased.

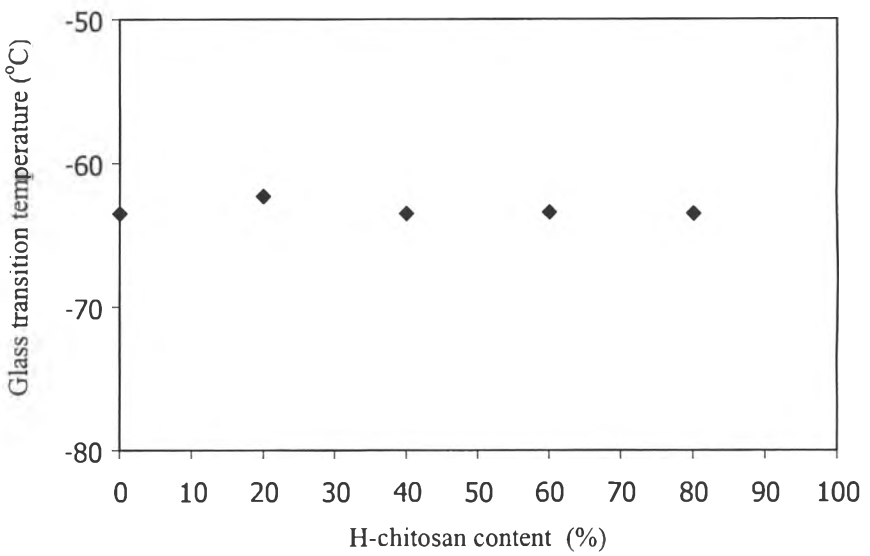

Figure 4.7 Glass transition temperature of H-chitosan/PCL blend films as a function of H-chitosan content.

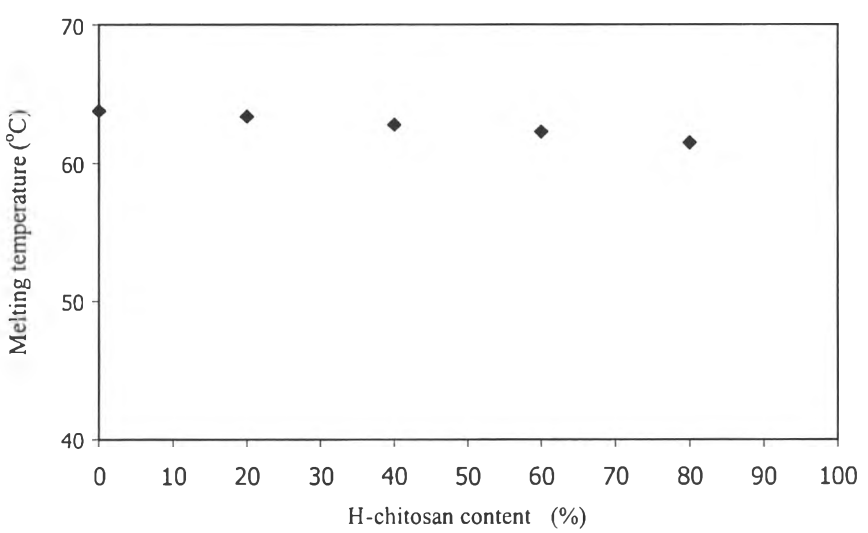

Figure 4.8 Melting temperature of H-chitosan/PCL blend films as a function of H-chitosan content.

These results indicate that the H-chitosan/PCL blend films are immiscible and corresponded to the result from SEM.

4.5 Thermal Stability

The decomposition temperatures (T_d) of pure H-chitosan, PCL, and H-chitosan/PCL blend films were determined by thermogravimetric analysis. Figure 4.9 (a) shows two T_ds of pure H-chitosan at 255.38°C and 321°C which corresponded to the T_d of hexanoyl groups (T_{d1}) and glycosidic linkage of chitosan (T_{d2}), respectively. Zong *et al.* (2000) investigated thermal properties of chitosan with a degree of deacetylation of 90%, H-chitosan, decanoyl chitosan (D-chitosan), and lauroyl chitosan (L-chitosan) by DSC measurement. It was found that the exothermic peaks of chitosan, H-, D-, and L-chitosan observed at 298°C, 225°C, 246°C, and 255°C, respectively, were their thermal decomposition temperatures. Grant *et al.* (1990) also reported that chitosan with degree of deacetylation of 86.4% and its lauroyl derivative had the exothermic decomposition peaks at 322°C and 217° C, respectively. These evidences suggested that the thermal stability of H-chitosan decreased when the hexanoyl groups were introduced to chitosan backbone.

Figure 4.9 (c), thermogravimetric thermogram of pure PCL film shows a strong peak at 391.08°C which is the decomposition temperature of ester linkage of PCL (T_{d3}).

For thermogravimetric thermogram of blend film with 40% H-chitosan content (Figure 4.9 (b)), two characteristic T_{d1}, T_{d2}, peaks of pure H-chitosan and characteristic T_{d3} peak of pure PCL were observed and found in all blend compositions. These peaks did not shift from the position when compared with the thermograms of pure H-chitosan and PCL films. These results suggest that the thermal stability of H-chitosan was not improved by blending with PCL.

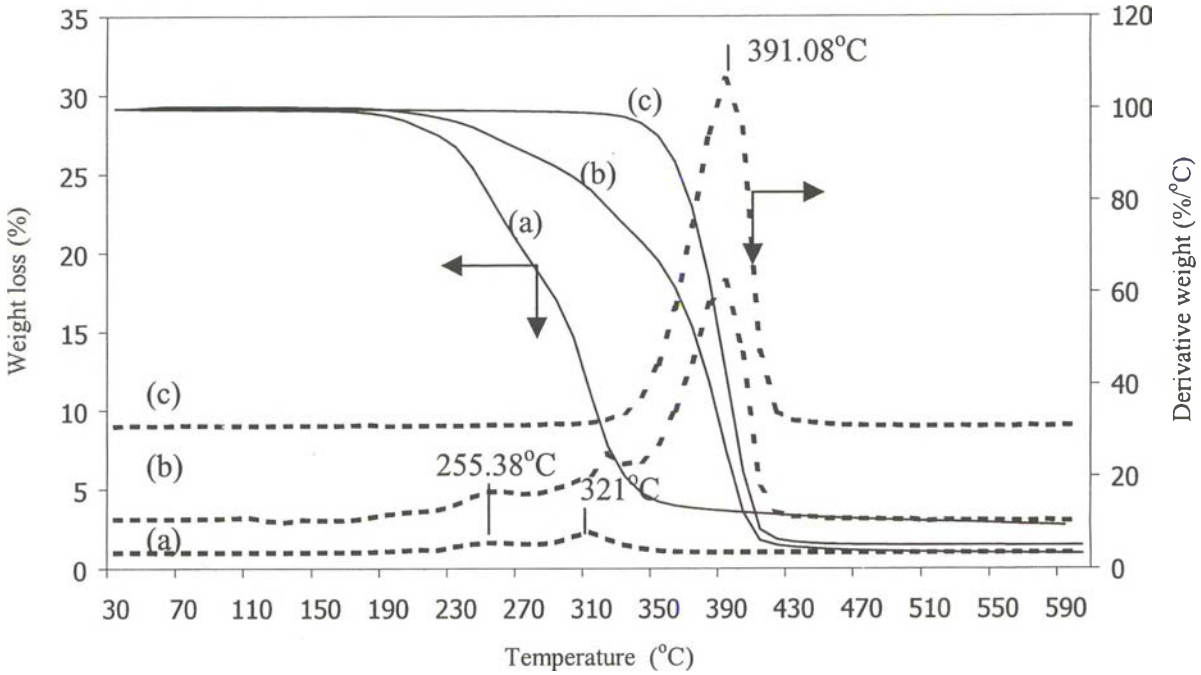

Figure 4.9 TGA thermograms of (a) H-chitosan; (b) blend with 40% H-chitosan; and (c) PCL films.

4.6 Crystalline Structure

WAXD pattern of pure H-chitosan is exhibited in Figure 4.10 (a). H-chitosan shows a strong diffraction peak at diffraction angles (2θ) of 2-6° together with a broad peak at diffraction angles (2θ) of 20°. Similar results have been reported by Zong *et al.* (2000), who synthesized and characterized the structure of acylated chitosans which were hexanoyl, decanoyl, and lauroyl chitosan, in which the acyl side chains were substituted at the pyranose ring of chitosan. They found that the *d*-spacing of diffraction angles (2θ) of 2-6° of each chitosan derivative increased as a function of the number of carbon atoms of acyl substituents. As a result, the side chains were packed with each other forming a layered structure with the main chains extended.

In Figure 4.10 (f), X-ray diffraction pattern of pure PCL shows two sharp diffraction peaks which appear at diffraction angles (2θ) of 21.4° and 23.9°. For the H-chitosan/PCL blends films, the diffraction patterns are shown in Figure 4.10 (b)-(e). There are the diffraction peaks at diffraction angles (2θ) of 21.5°, 23.8°, and 2-6°

which are the characteristic diffraction peaks of pure PCL and H-chitosan, respectively. When compared these three diffraction peaks with pure H-chitosan and PCL diffraction peaks, the shift of the peaks was not observed and no peaks other than those of H-chitosan and PCL were observed.

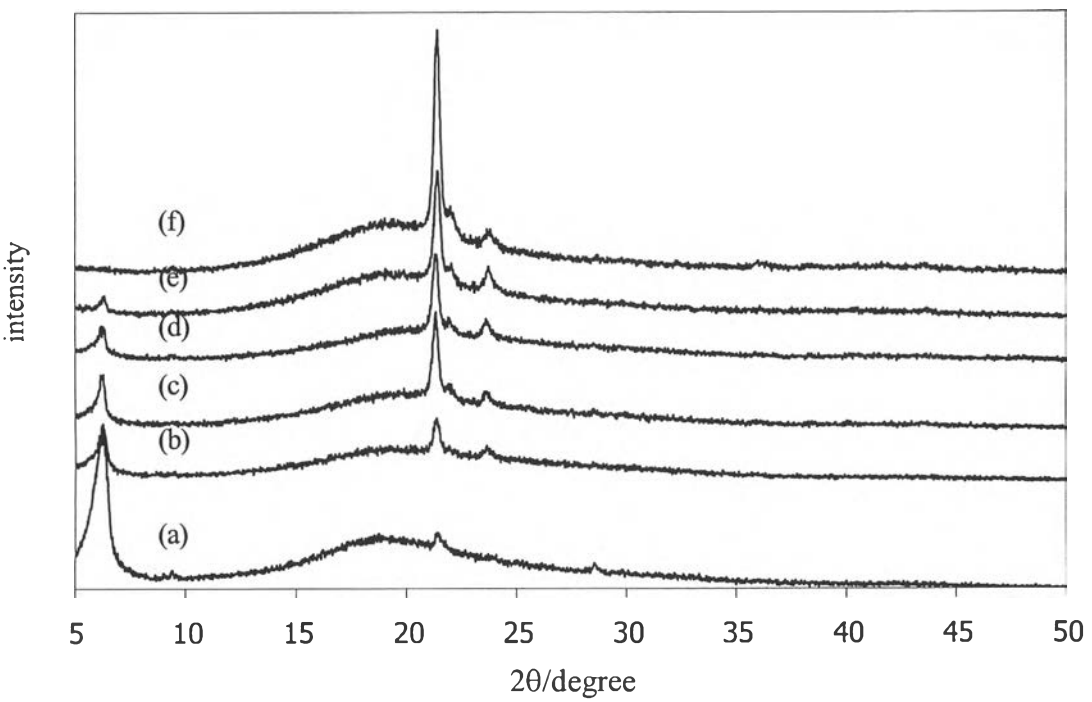

Figure 4.10 WAXD patterns of H-chitosan/PCL blend films. H-chitosan/ PCL blend composition: (a) 100/0 (H-chitosan); (b) 80/20; (c) 60/40; (d) 40/60; (e) 20/80; and (f) 0/100 (PCL).

Chiu and Min (2000) studied the microstructure of PCL crystals formed in PCL/PVC blends. They reported that the diffraction peaks of pure PCL appeared at diffraction angles (2θ) of 21.5° and 23.8° which are indexed to be (110) and (200) planes of an orthorhombic structure whereas the diffraction peak of PVC did not appear. For PCL/PVC blends, the diffraction peaks appeared at the position of pure PCL and the peak intensity increased as a function of PCL content. The result indicated that the crystal structure and unit cell dimensions of PCL crystals in the PCL/PVC blend remained the same as in pure PCL. In case of H-chitosan/PCL blends, the X-ray analysis indicates that an orthorhombic crystal form of PCL was not changed after blending with H-chitosan.

4.7 Mechanical Properties

Tensile strength and elongation at break of H-chitosan/PCL blend films as a function of H-chitosan content are illustrated in Figures 4.11 and 4.12, respectively. In Figure 4.11, the tensile strength of pure PCL and pure H-chitosan films were 12.21 MPa and 4.01 MPa, respectively. For the blend films, the tensile strength decreased dramatically with increasing H-chitosan content from 0% to 60%, and then slightly increased with increasing H-chitosan content from 60% to 100%. It was found that the minimum tensile strength of blend films was 2.69 MPa which was obtained at 60% H-chitosan content.

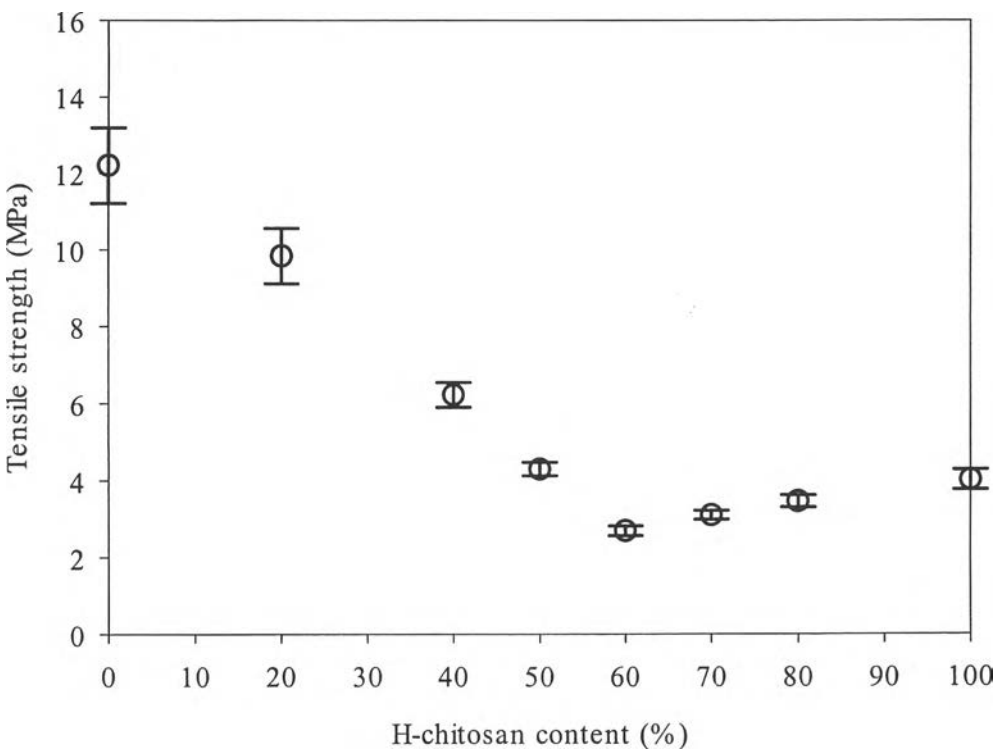

Figure 4.11 Tensile strength of H-chitosan/PCL blend films as a function of H-chitosan content.

Figure 4.12 shows the elongation at break of the blend films as a function of H-chitosan content. The elongation at break of pure PCL and pure H-chitosan films were 65.68% and 353.24%, respectively. For the blend films, the elongation at break increased with increasing the H-chitosan content from 0% to 40% and the minimum

value (29-30%) was obtained at 60-70% H-chitosan content. After that the elongation at break was slightly increased with increasing H-chitosan content.

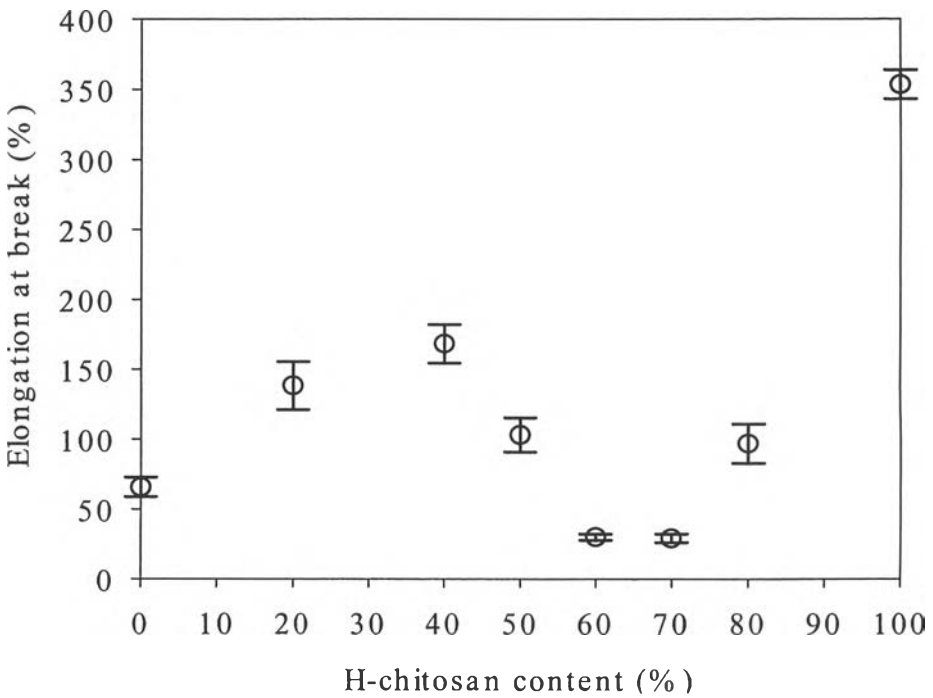

Figure 4.12 Elongation at break of H-chitosan/PCL blend films as a function of H-chitosan content.

This non-linear dependence of mechanical properties of the blend films on H-chitosan content supported the occurrence of phase separation occurred in the H-chitosan/PCL blend films. The poor mechanical properties of blend film with 60% H-chitosan content resulted from the agglomerate of PCL particles dispersed in H-chitosan matrix that were revealed in SEM micrographs and poor adhesion between H-chitosan matrix and PCL particle. Koenig and Huang (1995) explained the reason for a reduction of tensile strength of PCL/HA-CS blends that HA-CS has clumped or coalesced into larger aggregates when blended with PCL.

4.8 Oxygen Barrier Property

Figure 4.13 shows the oxygen permeability of blend films as a function of H-chitosan content. For pure PCL film, the oxygen permeability obtained was 782,055 $cm^3\mu m/m^2.sec.bar$ which was higher than the oxygen permeability of pure

H-chitosan film (186,173 $cm^3\mu m/m^2.sec.bar$). According to the report of Ng *et al.* (2000), the gas transport in PCL films occurred through the pores and defects in films because the O_2/N_2 permselectivity value obtained was similar to Knudsen permselectivity value of O_2/N_2.

In Knudsen flow, one type of the gas transport mechanism, the gas molecules permeate through defects in the polymer whose dimensions are comparable to or larger than the mean free path of the permeant molecules, in the range of 5-1000 A^o (Shilton *et al.*, 1996). Our SEM results have shown that the voids appeared on the surface of PCL film and have been consistent with the result of Ng *et al.* (2000).

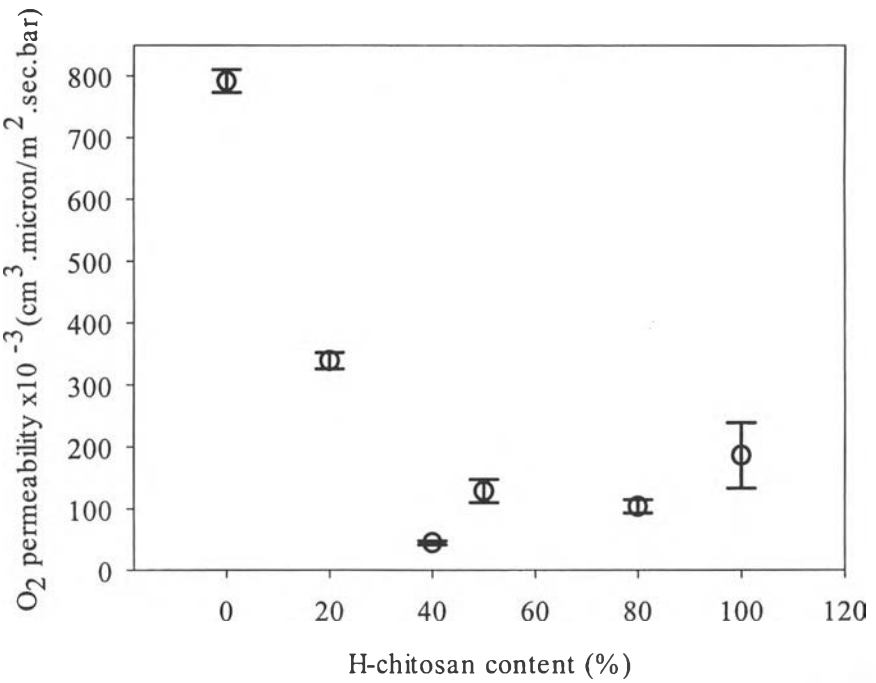

Figure 4.13 Oxygen permeability of H-chitosan/PCL blend films as a function of H-chitosan content.

For oxygen permeability of the blend films, it was found that oxygen permeability remarkably decreased when H-chitosan content increased from 0% to 40% and slightly increased from 40% to 100% H-chitosan content. The minimum oxygen permeability (44,628 $cm^3\mu m/m^2.sec.bar$) was obtained for the blend with 40% H-chitosan content. The decreasing of oxygen permeability resulted from H-chitosan particles dispersing in PCL matrix. These led to the difficulty of the

chitosan particles dispersing in PCL matrix. These led to the difficulty of the permeation oxygen gas through the blend films due to the gas pathways become more tortuous. Similar result was reported by Olabarrieta *et al.* (2001) who studied oxygen permeability of chitosan/PCL blend films. It was reported that oxygen permeability of chitosan/PCL blend films decreased compared with pure chitosan and PCL films. Consequently, the decreasing of oxygen permeability of PCL film indicates that oxygen barrier property of PCL was improved by blending with H-chitosan. By blending PCL with H-chitosan, it would be possible to use PCL in area where high oxygen barrier property was required.